Stem Cell Reports
Resource
OPEN ACCESS

Prospective Isolation and Comparison of Human Germinal Matrix and Glioblastoma EGFR$^+$ Populations with Stem Cell Properties

Jessica Tome-Garcia,[1,2] Rut Tejero,[2] German Nudelman,[3] Raymund L. Yong,[4] Robert Sebra,[5] Huaien Wang,[4] Mary Fowkes,[1] Margret Magid,[1] Martin Walsh,[5] Violeta Silva-Vargas,[6,7] Elena Zaslavsky,[3] Roland H. Friedel,[2] Fiona Doetsch,[6,7] and Nadejda M. Tsankova[1,2,*]

[1]Department of Pathology
[2]Department of Neuroscience, Friedman Brain Institute, Tisch Cancer Institute
[3]Department of Neurology
[4]Department of Neurosurgery
[5]Department of Pharmacological Sciences, Center for RNA Biology and Medicine and Tisch Cancer Institute
Icahn School of Medicine at Mount Sinai, New York, NY 10029, USA
[6]Department of Pathology and Cell Biology, Columbia University Medical Center, New York, NY 10032, USA
[7]Biozentrum, University of Basel, Basel 4056, Switzerland
*Correspondence: nadejda.tsankova@mssm.edu
http://dx.doi.org/10.1016/j.stemcr.2017.03.019

SUMMARY

Characterization of non-neoplastic and malignant human stem cell populations in their native state can provide new insights into gliomagenesis. Here we developed a purification strategy to directly isolate EGFR$^{+/-}$ populations from human germinal matrix (GM) and adult subventricular zone autopsy tissues, and from de novo glioblastoma (GBM) resections, enriching for cells capable of binding EGF ligand (^{LB}EGFR$^+$), and uniquely compared their functional and molecular properties. ^{LB}EGFR$^+$ populations in both GM and GBM encompassed all sphere-forming cells and displayed proliferative stem cell properties in vitro. In xenografts, ^{LB}EGFR$^+$ GBM cells showed robust tumor initiation and progression to high-grade, infiltrative gliomas. Whole-transcriptome sequencing analysis confirmed enrichment of proliferative pathways in both developing and neoplastic freshly isolated EGFR$^+$ populations, and identified both unique and shared sets of genes. The ability to prospectively isolate stem cell populations using native ligand-binding capacity opens new doors onto understanding both normal human development and tumor cell biology.

INTRODUCTION

Glioblastoma (GBM) is the most common and rapidly fatal adult brain tumor. Several developmental pathways important for the growth and proliferation of normal neural progenitors have been shown to be aberrantly reactivated in GBM and glioma stem cells (Canoll and Goldman, 2008; Chen et al., 2012; Lathia et al., 2015; Sanai et al., 2005), through complex genetic and emerging epigenetic alterations (Flavahan et al., 2016; Mack et al., 2015). Among these is the epidermal growth factor receptor (EGFR) pathway, with activating *EGFR* genomic alterations defining the most common "classical" GBM molecular signature (Brennan et al., 2013; Verhaak et al., 2010) and chromatin remodeling at its promoter driving *EGFR* overexpression (Erfani et al., 2015). EGFR is also highly expressed in the human developing germinal matrix (GM), as well as focally in the infant and adult subventricular zone (SVZ) (Erfani et al., 2015; Sanai et al., 2011; Weickert et al., 2000), but the stem cell properties and molecular characteristics of human EGFR-positive (EGFR$^+$) neural cells have not been well characterized nor compared with their EGFR$^+$ GBM counterparts, especially in populations derived from fresh human tissues. Here we prospectively isolated EGFR$^+$ cells from fresh GM, SVZ, and GBM human tissues, based on their ability to bind the cognate EGF ligand, which allowed us to directly compare their acute-state functional properties and whole-transcriptome signatures. We demonstrate that developing EGFR$^+$ GM, but not adult EGFR$^+$ SVZ, populations display proliferative stem cell properties in vitro. EGFR$^+$ GBM cells with ligand-binding capacity (^{LB}EGFR$^+$) recapitulate this developmental phenotype functionally in vitro, show capacity for tumor initiation in vivo, and share transcriptomes related to cell growth and cell-cycle regulation.

RESULTS

EGFR$^+$ Cells Isolated from Human GM Display Stem Cell Properties In Vitro

To better define the functional properties of EGFR-expressing cells during human brain development, we first characterized their immunophenotype in vivo in GM and SVZ human postmortem tissues. At 16–22 gestational weeks (gw), many but not all cells within the GM expressed EGFR (Figures 1A, S1, and S2). EGFR$^+$ cells near the ventricular surface displayed radial morphology, and sometimes co-stained with glial fibrillary acidic protein (GFAP), while those in the deeper GM layers frequently co-expressed

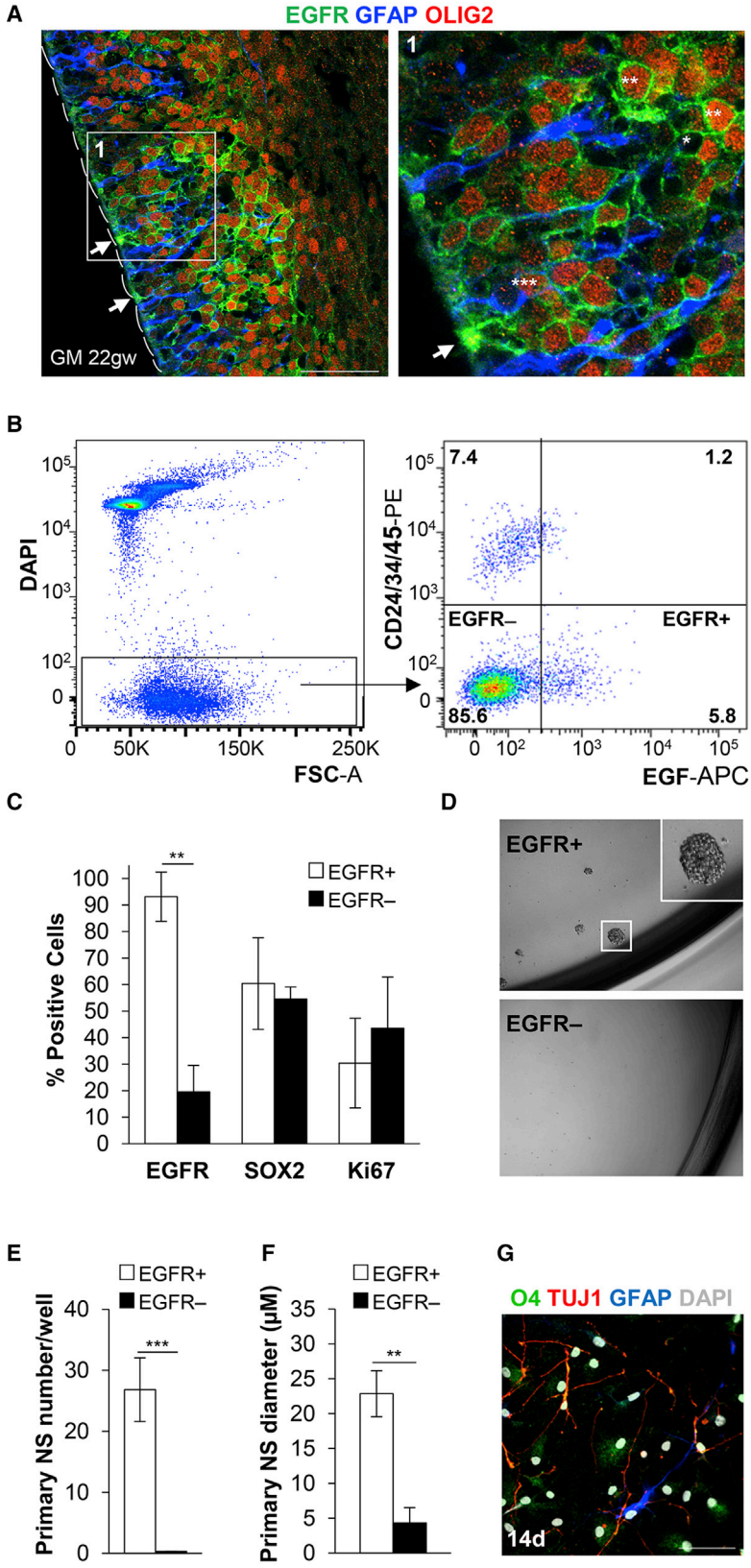

Figure 1. Human EGFR$^+$ GM Cells Isolated by FACS Display Stem Cell Properties In Vitro

(A) Immunofluorescence in human GM tissue shows many EGFR$^+$OLIG2$^+$ (**), scattered EGFR$^+$GFAP$^+$ OLIG2$^+$ (***), and exclusively EGFR$^+$ (*) cells, some of which show radial morphology (arrows) next to the developing ependyma (dashes) (see also Figures S1A–S1F and S2A).

(B) Representative FACS isolation of EGFR$^+$/EGFR$^-$ cells using EGF-APC for positive selection, and CD24/CD34/CD45-PE and DAPI for exclusion (GM, 21gw).

(C) Acute immunofluorescence of sorted GM EGFR$^{+/-}$ cells (2 hr after FACS) shows predominant distribution of EGFR in the positive fraction (93%) (**p = 0.002), and comparable expression of SOX2 and Ki67 in both fractions (n = 3 independent experiments) (see also Figure S2G).

(D) Representative primary NS growth at 6 days.

(E and F) Quantification of primary NS growth (n = 12 independent experiments; ***p = 2.9 × 10^{-5}) and (F) NS size (n = 5 independent experiments; **p = 0.01) at 6 days (EGF + FGF).

(G) Under differentiating conditions, EGFR$^+$-derived cells show tri-lineage differentiation toward astrocytic (GFAP$^+$), oligodendroglial (O4$^+$), and neuronal (TUJ1$^+$) fates (representative example of three independent samples).

Scale bars, 50 μm. Magnification of NS images, 10×. Bar graphs show mean ± SEM.

OLIG2 (Figures 1A and S2A). Both EGFR$^+$ and EGFR$^-$ cells expressed Ki67, as well as the stem cell markers SOX2 and Nestin (Figures S1A–S1F). To isolate human EGFR$^+$ and EGFR$^-$ populations from unfixed GM and SVZ dissections, we adapted a mouse fluorescence-activated cell sorting (FACS) strategy, which selects for EGFR$^+$ cells based on their native binding to EGF ligand, while simultaneously excluding ependymal cells, endothelium, and inflammatory cells (Figures 1B, S2D, S2H, and S2I; Ciccolini et al., 2005; Codega et al., 2014; Pastrana et al., 2009). Acute immunostaining of the sorted populations from GM tissues demonstrated EGFR expression in more than 93% of cells within the EGFR$^+$ fraction and a similar co-expression pattern of SOX2 and Ki67 as was observed in vivo (Figures 1C and S2G).

We then functionally characterized the in vitro stem cell properties of the freshly isolated EGFR$^+$ and EGFR$^-$ populations, by examining their ability to form proliferative and self-renewing neurospheres (NS) and their potency for tri-lineage differentiation. Under standard NS medium conditions with EGF + fibroblast growth factor (FGF) ligand supplementation, EGFR$^+$ cells (EGFR$^+$ DAPI$^-$CD24$^-$CD34$^-$CD45$^-$) isolated from prenatal GM showed NS formation by 6 days (Figures 1D–1F) and could be passaged serially (Figures S2D and S2F). To assess whether our ligand-binding isolation strategy selects for proliferating cells dependent on EGF for growth, we also cultured EGFR$^+$ cells in the absence of exogenous EGF, supplementing the medium with FGF only or without any ligand. FACS-isolated EGFR$^+$ cells showed similar number of primary NS with EGF + FGF, FGF only, and in the absence of any ligand, and formed self-renewing NS in the absence of EGF (Figure S2F). EGFR expression was maintained during NS passaging, including in clonal NS derived from single-cell seeding (1 cell/well) (Figure S1G). Under differentiation conditions, only EGFR$^+$ GM-derived NS showed potential for tri-lineage differentiation (Figures 1G and S2D). In contrast, EGFR$^-$ cells (EGFR$^-$DAPI$^-$CD24$^-$CD34$^-$CD45$^-$) showed little or no NS proliferation, and lacked the capacity for self-renewal in serial passaging (Figures 1D–1F, S2D, and S2E). We also studied the properties of EGFR$^+$ cells in the infant and adult human SVZ. Immunofluorescence revealed focal and weaker EGFR expression in the postnatal SVZ in vivo, with drastic decline in Ki67 cell-cycle labeling (Figures S1H, S2B, and S2C), consistent with previous reports (Erfani et al., 2015; Sanai et al., 2011). Accordingly, EGFR$^+$ cells isolated from infant SVZ gave rise to primary NS only (Figure S2H), and adult SVZ EGFR$^+$ cells did not show any growth (n = 10) (Figure S2I). Therefore, EGFR$^+$ populations derived acutely from human GM encompassed the cells with in vitro stem cell properties.

EGFR$^+$ GBM Populations with Ligand-Binding Capacity Display Stem Cell Properties In Vitro

To assess whether EGFR$^+$ cells in freshly dissociated GBM samples also exhibit stem cell properties in vitro, we employed the same isolation methodology and culture conditions used for normal neural tissues. All GBM samples were de novo resections, with different genomic alterations, including *EGFR* amplification and/or chromosome 7 polysomy, *EGFRvIII* mutation, and isocitrate dehydrogenase 1 (IDH1) mutation (Table S1). In vivo analysis of EGFR expression in these GBM samples revealed widespread expression of its intracellular domain (EGFR-ID) and more variable expression of its extracellular domain (EGFR-ED), consistent with EGFR-ED's focal loss in *EGFRvIII* and/or other truncating mutations (Figure 2A; Brennan et al., 2013). Expression of SOX2 and Nestin in GBM resembled the immunophenotype seen during GM development (Figures S1I–S1K).

In contrast to GM, GBM FACS revealed two populations of EGFR$^+$ cells. The main population (defined here as EGFR$^+$ DAPI^{low}) showed a unique shift in DAPI fluorescence and greater forward scatter (Figures 2B [right] and S3B). The minor EGFR$^+$ population was DAPI$^-$ (Figure 2B, left), similar to that in GM. qRT-PCR analysis revealed that ligand-binding *EGFR-ED* transcript is significantly overexpressed in EGFR$^+$DAPI^{low} populations only, while *EGFR-ID* and *EGFRvIII* were variable (Figure 2C). This suggested that our technique is selective for cells with preserved EGF ligand-binding ability and *EGFR-ED* expression (annotated hereafter as ^{LB}EGFR$^+$), regardless of their EGFRvIII status.

We next assessed the ability of each different GBM FACS-purified population to grow and form self-renewing gliomaspheres (GS) in vitro. Similar to GM, GBM GS only arose from ^{LB}EGFR$^+$ populations (Figure 2D), with ^{LB}EGFR$^+$ DAPI^{low} cells forming more and larger primary GS than ^{LB}EGFR$^+$DAPI$^-$ cells at 12 days (Figure 2E, n = 16), and were the only ones to show self-renewal in serial passaging (Figures 2D and 2E). In contrast, EGFR$^-$DAPI$^-$ cells did not divide (Figure S3B) and EGFR$^-$DAPI^{low} cells divided initially in one sample only, but did not form GS even after 4 weeks of growth (Figures 2D and 2E). Importantly, populations from our exclusion channels, CD24-PE, CD34-PE, and CD45-PE, cultured under identical conditions, attached to the plate but did not proliferate into GS (Figure S3D). As with GM, sphere formation in ^{LB}EGFR$^+$ DAPI^{low} glioma cells was not dependent on EGF being present in the culture medium. ^{LB}EGFR$^+$DAPI^{low} GBM populations formed similar numbers of primary and self-renewing GS under EGF + FGF, FGF only, and no ligand conditions (Figures 2F, S2J, and S2K). They also displayed capacity for tri-lineage differentiation (Figures 2G and 2H). Extreme limiting dilution analysis (ELDA) revealed comparable

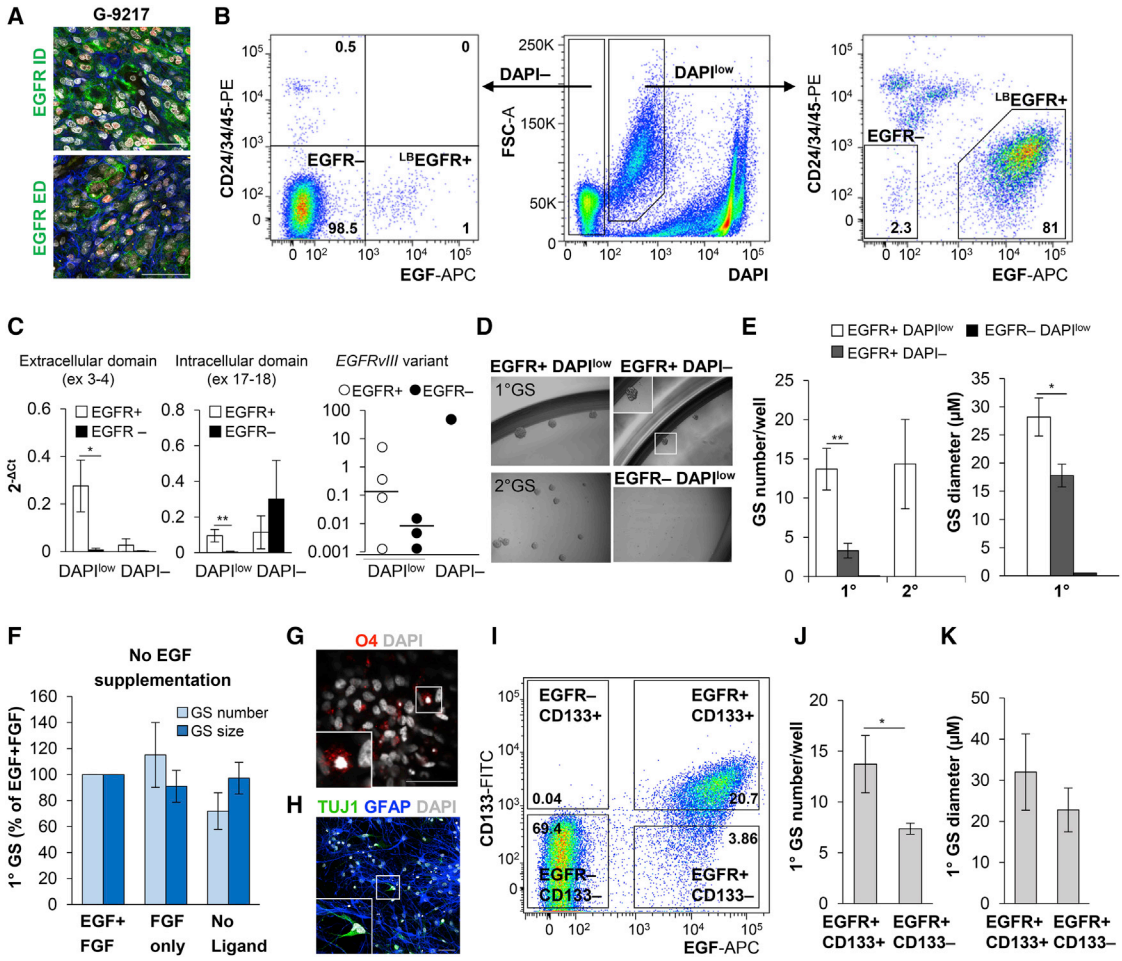

Figure 2. FACS-Isolated GBM ^{LB}EGFR^{+} Populations Display Stem Cell Properties In Vitro and Encompass All Sphere-Forming Cells

(A) Representative GBM specimen showing widespread expression of intracellular domain (ID) and focal expression of extracellular domain (ED) of EGFR, with co-localization for GFAP (blue) and OLIG2 (red).

(B) Cell sorting based on EGF binding allows the purification of EGFR^{+} cells with ligand-binding capacity (^{LB}EGFR^{+}) from fresh GBM samples, while excluding non-neoplastic endothelium and inflammatory cells (CD24^{+}/CD34^{+}/CD45^{+}-PE) and dead cells (high DAPI^{+}, 10^{4}–10^{5}). A significant fraction of ^{LB}EGFR^{+} live cells shows a distinct forward scatter shift (FSC-A) and dim DAPI fluorescence (DAPI^{low}) (see also Figure S3B).

(C) qRT-PCR confirms selectivity for *EGFR* with intact ligand-binding *ED* transcript (exons 3–4) in the positive fraction (^{LB}EGFR^{+}) (*p = 0.049; n = 3 independent experiments). *EGFR-ID* transcript (exons 17–18) and mutant *EGFRvIII* transcript (exons 1–8 junction) are variably present in both fractions (n = 3 independent experiments; **p = 0.009).

(D) GS formation is seen exclusively in ^{LB}EGFR^{+} populations (day 12).

(E) GS derived from ^{LB}EGFR^{+}DAPI^{low} cells are more numerous than ^{LB}EGFR^{+}DAPI^{-} cells (**p = 0.003) and larger in size (*p = 0.05) (n = 16 independent experiments). Only ^{LB}EGFR^{+}DAPI^{low} cells form secondary (2°) GS (day 12) (n = 10 independent experiments).

(F) ^{LB}EGFR^{+}DAPI^{low} cells form similar number and size of 1° GS when cultured with EGF + FGF, FGF only, or without any ligand (n = 3 independent experiments) (see also Figures S2J and S2K).

(G and H) EGFR^{+} GS show the ability for multipotent lineage differentiation (representative example from three independent tumors).

(I–K) Combined FACS for CD133 and EGFR shows both CD133^{+} and CD133^{-} GS-forming populations to be EGFR^{+} (I), with greater number of GS derived from ^{LB}EGFR^{+}CD133^{+} cells (*p = 0.03) (n = 3 independent experiments) (J), of equal size to ^{LB}EGFR^{+}CD133^{-} cells (K) (n = 3 independent experiments; 12 days) (see also Figure S3C).

Scale bars, 50 μm. Magnification of GS images, 10×. Bar graphs show mean ± SEM.

stem cell frequencies in GM and GBM ^{LB}EGFR^{+} populations, regardless of whether EGF was added to the culture medium (Table S2). Expression of EGFR was maintained in clonogenic spheres (1 cell/well) (Figure S1N), and was upregulated in GS formed without exogenous EGF in the culture medium (Figure S1O).

Of note, two GBM samples in our study did not show any expression of EGFR, and thus also lacked a defined ^{LB}EGFR^{+} population. In one of them, G-10416, GS formations were present in the EGFR^{-} tumor population (Figure S2L) while in the other, G-11702, GS were not formed (data not shown). Overall, the data indicate that for GBM tumors that express EGFR, with or without *EGFR* amplification/vIII mutation, EGF-based isolation enriches for ^{LB}EGFR^{+} populations with in vitro stem cell properties.

Sphere-Forming Cells Are Fully Captured within ^{LB}EGFR^{+} GBM Populations

To further validate our technique, we compared EGF-based FACS against several established glioma stem cell isolation markers, including CD133 (Prominin-1), CD171 (L1CAM), CD44, and CD140a (PDGFRA) (Anido et al., 2010; Bao et al., 2008; Flavahan et al., 2016; Singh et al., 2004). Simultaneous sorting with CD133 and EGF revealed three main populations: ^{LB}EGFR^{+}CD133^{+}, ^{LB}EGFR^{+}CD133^{-}, and EGFR^{-}CD133^{-} (Figures 2I, S3A, and S3B). Upon culturing, GS formation was seen in ^{LB}EGFR^{+}CD133^{+} and ^{LB}EGFR^{+}CD133^{-} populations, the former being more numerous, consistent with previous reports (Figures 2J and 2K; Beier et al., 2007). No GS were present in EGFR^{-}CD133^{-} cells (Figure S3B). Again, GS grew in similar numbers with and without the addition of exogenous EGF to the medium (Figure S3C). Similarly to CD133, ^{LB}EGFR^{+} GBM cells were present within both positive and negative CD171, CD140a, and CD44 populations, encompassing all sphere-forming populations (Figures S3E–S3G). These results underscore the utility of our ligand-based methodology for the selective yet inclusive isolation of glioma cells with in vitro proliferative stem cell properties from fresh EGFR-expressing GBM tumors, capturing all sphere-forming populations.

Transplanted ^{LB}EGFR^{+}DAPI^{low} GBM Cells Display Robust Tumorigenic Abilities In Vivo

To test the tumorigenic capacity of purified ^{LB}EGFR^{+} GBM cells in vivo, we injected acutely sorted ^{LB}EGFR^{+}DAPI^{low}, EGFR^{-}DAPI^{low}, ^{LB}EGFR^{+}DAPI^{-}, and EGFR^{-}DAPI^{-} cells, without any prior culture, intracranially into 2-month-old immunocompromised mice, and assessed their ability for tumor initiation at an early, subclinical time point of 60 days. Only ^{LB}EGFR^{+}DAPI^{low} populations showed capacity for tumor initiation, displaying robust proliferation (60% HNA^{+}Ki67^{+} co-localization) (Figures 3A and 3B) and migration along striatal white matter fibers (Figure 3A). In contrast, mice transplanted with EGFR^{-}DAPI^{low}, EGFR^{-}DAPI^{-}, or ^{LB}EGFR^{+}DAPI^{-} cells showed minimal proliferation in one case only of EGFR^{-}DAPI^{low} transplantation (Figure 3C) or no engraftment (Figures 3D and 3E). By 4–6 months, mice injected with ^{LB}EGFR^{+}DAPI^{low} cells exhibited large and diffusely infiltrative high-grade gliomas (Figure 3F), retaining the *EGFR* amplification status of their original resection (Figure 3G). The phenotype in the well-formed tumors at 4–6 months was less proliferative than at 2 months (Figure 3B), with expression of differentiating markers such as GFAP and TUJ1 (TUBB3) (Figure 3H), recapitulating human GBM heterogeneity (Figures S1L and S1M). Overall, these results demonstrate that ^{LB}EGFR^{+}DAPI^{low} GBM cells not only define sphere-forming populations in vitro but are also capable of tumor initiation and diffuse migration in vivo, underscoring the utility of EGFR-binding capacity as a powerful approach to isolate GBM populations with tumorigenic properties.

Comparative Transcriptome Profiling of ^{LB}EGFR^{+} GM and GBM Populations

To define the transcriptional signature in our FACS-purified human germinal matrix and glioma-derived EGFR^{+} populations, we performed deep transcriptome sequencing analysis via RNA sequencing (RNA-seq) on acutely isolated ^{LB}EGFR^{+} and EGFR^{-} GM and GBM (DAPI^{low}) populations. Developing GM EGFR^{+} and EGFR^{-} transcriptomes appeared most similar to one another by hierarchical clustering and principal component analysis, and interestingly, GBM ^{LB}EGFR^{+} transcriptomes were more similar to GMs than to their neoplastic EGFR^{-} counterpart (Figures 4A and S4A). Differential expression analysis revealed well-defined large subsets of upregulated and downregulated genes between GBM ^{LB}EGFR^{+} and EGFR^{-} populations, and smaller ones between GM EGFR^{+} and EGFR^{-} populations (Figure 4B). Differential gene set analysis revealed strong enrichment in pathways related to cell proliferation and mitotic cell cycle in both GM and GBM ^{LB}EGFR^{+} populations (Figures S4B–S4D and Table S3). Further analysis defined subset of 50 developmentally regulated genes to be uniquely shared between human GBM and GM EGFR^{+} populations, including several implicated in cell-cycle regulation: *CENPE*, *DBF4*, *KPNA2*, and *KNSTRN* (Figures 4C–4E and Table S3).

Together, our data provide functional and molecular evidence for stem cell properties in ligand-binding EGFR^{+} cells during both neural development and in GBM.

DISCUSSION

Comparative analyses of non-neoplastic and neoplastic human neural populations, isolated ex vivo from fresh pathology samples, are technically challenging but can yield important insight into both normal biology and gliomagenesis. Here we provide a useful ligand-based methodology to purify EGFR^{+} GM progenitors and GBM cells from fresh human tissues, and elaborate on their phenotypic,

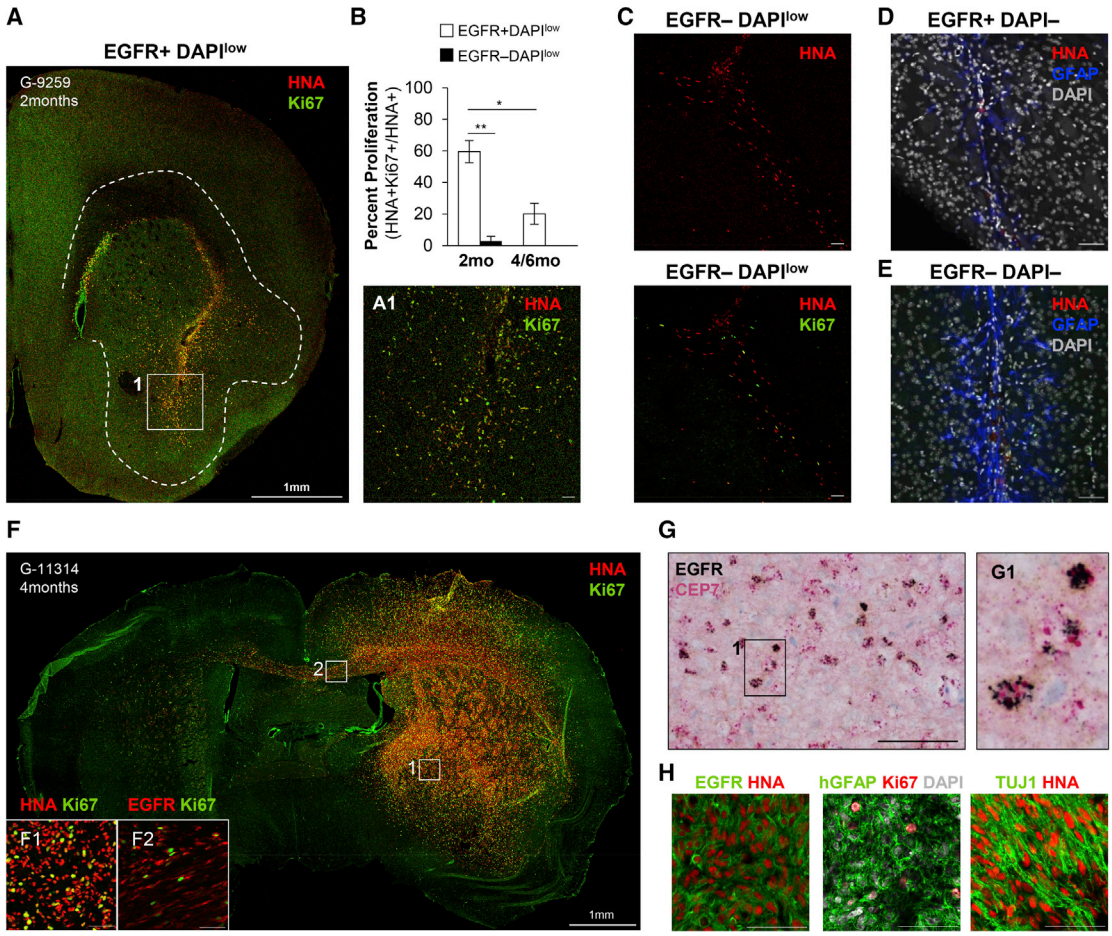

Figure 3. Transplanted ^{LB}EGFR^{+} GBM Cells Are Robustly Tumor-Initiating In Vivo

(A) Intracranial xenotransplantation yields robust tumor growth and infiltration at 60 days in ^{LB}EGFR^{+}DAPI^{low} populations only (1 × 10^{5}).

(B) Quantification of proliferation (Ki67^{+}) in human nuclear antigen (HNA^{+}) glioma cells from ^{LB}EGFR^{+}DAPI^{low} and EGFR^{-}DAPI^{low} transplantations (**p = 0.001 at 2 months, *p = 0.014 at 4–6 months) (n = 3 independent experiments).

(C) EGFR^{-}DAPI^{low} (1 × 10^{5}) glioma cells show no or minimal proliferation close to the needle track at 60 days (n = 3 tumors; example shown is the only one with minimal proliferation).

(D and E) ^{LB}EGFR^{+}DAPI^{-} (0.5 × 10^{5}) and EGFR^{-}DAPI^{-} (1 × 10^{5}) populations show only debris around the needle track surrounded by a GFAP^{+} astroglial scar at 60 days (representative examples of three independent tumors).

(F–H) Four to six months after injection, ^{LB}EGFR^{+}DAPI^{low} (1 × 10^{5}) transplants display large and diffusely infiltrative high-grade gliomas, (G) retain *EGFR* amplification status by chromogenic in situ hybridization, and (H) express EGFR as well as differentiating markers GFAP and TUJ1 (representative examples, n = 3 independent tumors for F–H).

Scale bars, 50 μm. Bar graphs show mean ± SEM.

functional, and molecular comparative properties. Importantly, we discover that EGFR^{+} GM and GBM populations encompass all sphere-forming cells in vitro, displaying self-renewal and multi-lineage differentiation stem cell properties, and that freshly isolated ^{LB}EGFR^{+} GBM cells form high-grade and diffusely infiltrating gliomas by 4 months after orthotopic transplantation. We confirm that this ligand-based isolation strategy does not simply select for populations dependent on EGF ligand for growth, demonstrating the ability of ^{LB}EGFR^{+} populations for sphere formation in vitro and tumor initiation in vivo in the absence of exogenous EGF ligand supplementation.

Several important markers have been utilized to identify and characterize glioma stem cells (GCS) in fresh human GBM tissues and patient-derived neurosphere cultures, but many of them have not captured all sphere-forming cells in vitro (Lathia et al., 2015). By combining our EGF ligand-based isolation methodology with CD133, CD140a, CD171, or CD44, we show that EGF ligand binding captures all GS-forming colonies. This underscores the

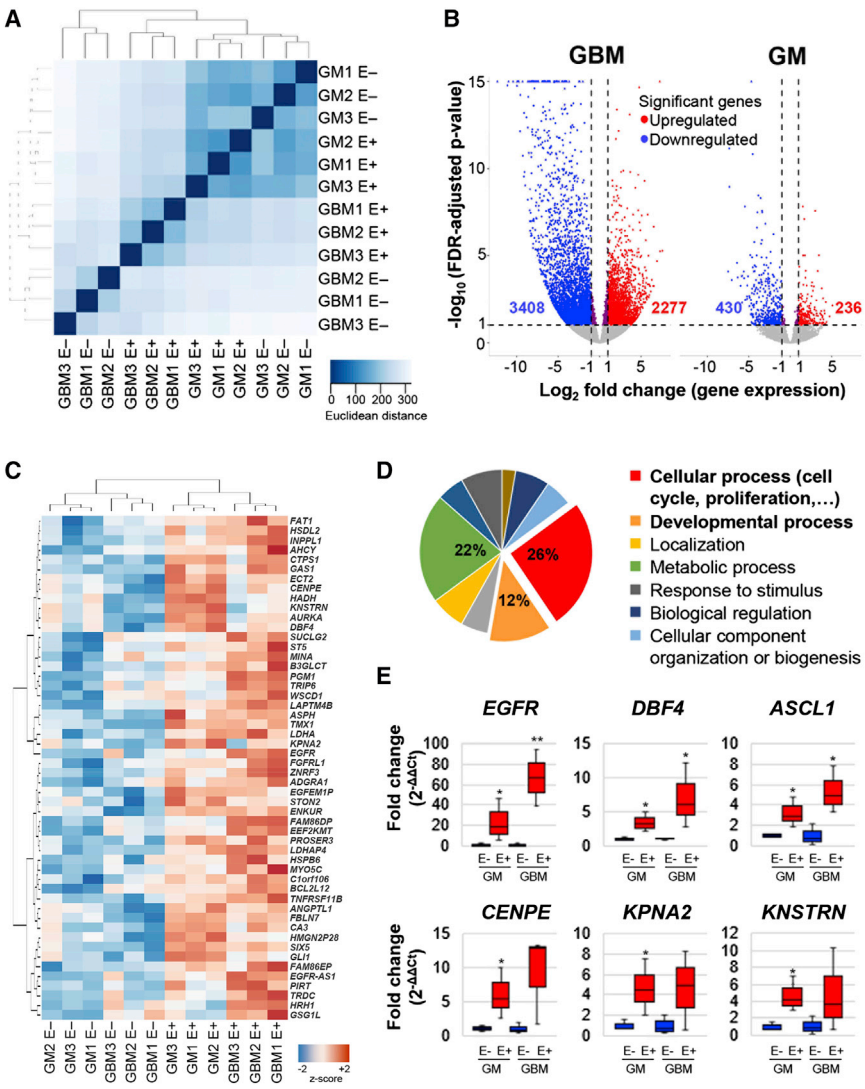

Figure 4. Differential Transcriptome Analysis of EGFR$^+$ GM and GBM Populations Defines a Shared Gene Set

(A) Unsupervised hierarchical clustering of whole-transcriptome RNA-seq data, using Euclidean distance as the metric, of acutely isolated EGFR$^+$/EGFR$^-$ populations from three GM (19–22 gw) and three GBM independent samples, shows higher resemblance of ^{LB}EGFR$^+$ GBMs with GMs than with EGFR$^-$ GBMs (see also Figure S4A).

(B) Differential gene expression analysis in ^{LB}EGFR$^+$ versus EGFR$^-$ populations, performed independently for all three GBM and GM samples, defines a subset of significantly upregulated and downregulated genes in both datasets.

(C–E) Analysis of the intersection between the two upregulated gene datasets (2,277 and 236, red) in EGFR$^+$ GM and GBM. (C) Heatmap of row-normalized expression values for upregulated shared genes (false discovery rate adjusted $p < 0.1$, $z = [x - \text{mean}]/SD$) (see also Table S3). (D) Pie chart depicts distribution of top biological processes in the shared gene set, analyzed by PANTHER database. (E) Validation of gene expression by qRT-PCR in upregulated EGFR$^+$ GM/GBM genes related to cell proliferation ($n = 3$ independent experiments). Plots show the median (black horizontal line), 25th and 75th percentiles (boxes), and range (whiskers) of the data. One-tailed unpaired Students' t test and Mann-Whitney U test for non-parametric test were used to calculate statistical significance (*EGFR* GM, *p = 0.024, GBM, **p = 0.007; *DBF4* GM, *p = 0.023, GBM, *p = 0.046; *ASCL1* GM, *p = 0.03, GBM, *p = 0.02; *CENPE* GM, *p = 0.039; *KPNA2* GM, *p = 0.04; *KNSTRN* GM, *p = 0.02).

ability of our EGF ligand-based isolation methodology to recapitulate the in vitro GSC phenotypes previously characterized by others, as well as to capture additional sphere-forming populations with potential functional and molecular significance.

Although GBM tumors with diffuse *EGFR* amplification displayed the most pronounced ^{LB}EGFR$^+$ population in FACS, we also captured all sphere-forming cells in EGFR-expressing GBM tumors without *EGFR* amplification (7 out of 19), one of which harbored IDH1 mutation. Thus, we believe this methodology will be useful for isolating stem cell populations in both EGFR-amplified "classical" and IDH1-mutant "proneural" GBM tumors, and perhaps others, as long as they express EGFR, but may not be applicable for occasional tumors that lack a defined ^{LB}EGFR$^+$ population. Given the bias of neurosphere assays and xenograft tumor initiation models for proliferation, our methodology is particularly useful for isolating populations with active, but not necessarily quiescent, stem cell properties.

The similarities between the transcriptome of GM and GBM ^{LB}EGFR$^+$ stem cell populations for markers of cell-cycle regulation suggest that the proliferative tumor phenotype of ^{LB}EGFR$^+$ GBM populations may be at least partially driven by co-opted transcriptional programs important for cell division during germinal matrix development (Flavahan et al., 2016; Liu et al., 2015; Mack et al., 2015; Suva et al., 2014; Tsankova and Canoll, 2014). The interplay

between genomic alterations and developmental remodeling of transcriptional networks in tumor cells is an intriguing question to be explored in future studies, and to this end we have here validated a useful and clinically relevant methodology for the prospective isolation of neural and GBM populations with proliferative stem cell properties.

EXPERIMENTAL PROCEDURES

Detailed methods are provided in Supplemental Experimental Procedures.

Sample Collection

All specimen collection was performed de-identified in accordance with the policies and regulation at the Icahn School of Medicine at Mount Sinai (ISMMS) and its institutional review board (IRB#AAAJ9652-Y1M00, HS#14-01007).

Fluorescence-Activated Cell Sorting

Single-cell suspension was obtained from fresh tissue (dissected GM/SVZ autopsy or GBM surgical material) by mechanical and enzymatic papain dissociation, and incubated with EGF-Alexa Fluor 647(APC) complex for positive selection of EGFR cells (1 μg per 10^6 live cells), and with CD24/CD34/CD45 antibodies and DAPI for exclusions (Codega et al., 2014).

Cell Culture

Cells were cultured on 96-well low-adherence plates in freshly made NS medium (see recipe in Supplemental Experimental Procedures), with addition of EGF (20 ng/mL) and/or basic FGF (bFGF) (20 ng/mL), or with no ligand, at a density of 10 cells/μL or 1 cell/μL (for 1° or 2° NS/GS formation, respectively). For ELDA, acutely sorted cells were seeded at 1, 10, 50, and 100 cells/well. For differentiation, NS/GS were seeded on PDL/laminin-coated coverslips and grown in NS medium without B27, EGF, and bFGF for 14 days.

Orthotopic Transplantation

Mouse studies were performed in accordance with the Institutional Animal Care and Use Committee (IACUC), protocol number IACUC-2014-0183. Acutely FACS-sorted cells ($0.5–1 \times 10^5$) from fresh GBM samples were injected into the striatum of 2-month-old SCID male mice (2 mm right lateral to bregma and 3 mm deep). Mice were euthanized for histological examination of tumor initiation at 60 days and of endpoint tumor formation when clinically symptomatic.

Gene Expression Analysis

Whole-transcriptome analysis was performed by RNA-seq on RNA extracted from freshly FACS-sorted $EGFR^{+/-}$ GBM and GM cells (125 bp pair-end sequencing, 38–50 million paired-end reads/sample, on Illumina HiSeq 2500). cDNA was generated using Clontech SMART-seq v4 (634888) and libraries using Nextera XT (FC-131-1024). The expression of selected genes was validated by qRT-PCR.

Immunofluorescence

Floating vibratome sections (40–60 μm), formalin-fixed paraffin-embedded (FFPE) sections (4 μm), NS/GS, and acutely fixed FACS-sorted cells were blocked in 10% normal donkey serum for 0.5–1 hr, incubated with primary antibody overnight at 4°C, incubated with secondary antibodies for 2–4 hr at room temperature, and visualized on a confocal Zeiss LSM710 microscope. Modified protocols were used for EGFR and O4 staining (see Supplemental Experimental Procedures).

ACCESSION NUMBERS

The accession number for the RNA-seq data reported in this paper is GEO: GSE96682.

SUPPLEMENTAL INFORMATION

Supplemental Information includes Supplemental Experimental Procedures, four figures, and three tables and can be found with this article online at http://dx.doi.org/10.1016/j.stemcr.2017.03.019.

AUTHOR CONTRIBUTIONS

Conception of project: F.D. and N.M.T. Experimental design and data interpretation: J.T.-G. and N.M.T. Development of EGF FACS technique: V.S.-V., F.D., J.T.-G., and N.M.T. In vitro assays, library preparation, qPCR, and histology: J.T.-G. Orthotopic transplantations: R.T. and R.H.F. Sequencing and bioinformatics: G.N., E.Z., M.W., and R.S. Tissue procurement: H.W., R.L.Y., M.M., M.F., and N.M.T. Manuscript preparation: J.T-G., F.D., and N.M.T. Editing: all authors. R.T. and G.N. contributed equally.

ACKNOWLEDGMENTS

We thank members of the Pathology Department and Biorepository Core (director M. Donovan) at ISMMS for facilitating tissue collection and procurement; the ISMMS Flow Cytometry CORE for expert advice and accommodation of fresh human tissue sorts 24hr/day; members of the F.D., J. Goldman, and J. Silva laboratories for assistance with reagents and equipment; P. Codega for advice on NS differentiation; H. Zou for scientific advice; and G. Petrov and M. Olabarria for graphical assistance. The research was supported by Mount Sinai seed grant funds (N.M.T., R.H.F.) and R01NS092735 (R.H.F.).

Received: July 14, 2016
Revised: March 17, 2017
Accepted: March 17, 2017
Published: April 20, 2017

REFERENCES

Anido, J., Saez-Borderias, A., Gonzalez-Junca, A., Rodon, L., Folch, G., Carmona, M.A., Prieto-Sanchez, R.M., Barba, I., Martinez-Saez, E., Prudkin, L., et al. (2010). TGF-beta receptor inhibitors target the CD44(high)/Id1(high) glioma-initiating cell population in human glioblastoma. Cancer Cell *18*, 655–668.

Bao, S., Wu, Q., Li, Z., Sathornsumetee, S., Wang, H., McLendon, R.E., Hjelmeland, A.B., and Rich, J.N. (2008). Targeting cancer stem cells through L1CAM suppresses glioma growth. Cancer Res. *68*, 6043–6048.

Beier, D., Hau, P., Proescholdt, M., Lohmeier, A., Wischhusen, J., Oefner, P.J., Aigner, L., Brawanski, A., Bogdahn, U., and Beier, C.P. (2007). CD133(+) and CD133(-) glioblastoma-derived cancer stem cells show differential growth characteristics and molecular profiles. Cancer Res. *67*, 4010–4015.

Brennan, C.W., Verhaak, R.G., McKenna, A., Campos, B., Noushmehr, H., Salama, S.R., Zheng, S., Chakravarty, D., Sanborn, J.Z., Berman, S.H., et al. (2013). The somatic genomic landscape of glioblastoma. Cell *155*, 462–477.

Canoll, P., and Goldman, J.E. (2008). The interface between glial progenitors and gliomas. Acta Neuropathol. *116*, 465–477.

Chen, J., McKay, R.M., and Parada, L.F. (2012). Malignant glioma: lessons from genomics, mouse models, and stem cells. Cell *149*, 36–47.

Ciccolini, F., Mandl, C., Holzl-Wenig, G., Kehlenbach, A., and Hellwig, A. (2005). Prospective isolation of late development multipotent precursors whose migration is promoted by EGFR. Dev. Biol. *284*, 112–125.

Codega, P., Silva-Vargas, V., Paul, A., Maldonado-Soto, A.R., Deleo, A.M., Pastrana, E., and Doetsch, F. (2014). Prospective identification and purification of quiescent adult neural stem cells from their in vivo niche. Neuron *82*, 545–559.

Erfani, P., Tome-Garcia, J., Canoll, P., Doetsch, F., and Tsankova, N.M. (2015). EGFR promoter exhibits dynamic histone modifications and binding of ASH2L and P300 in human germinal matrix and gliomas. Epigenetics *10*, 496–507.

Flavahan, W.A., Drier, Y., Liau, B.B., Gillespie, S.M., Venteicher, A.S., Stemmer-Rachamimov, A.O., Suva, M.L., and Bernstein, B.E. (2016). Insulator dysfunction and oncogene activation in IDH mutant gliomas. Nature *529*, 110–114.

Lathia, J.D., Mack, S.C., Mulkearns-Hubert, E.E., Valentim, C.L., and Rich, J.N. (2015). Cancer stem cells in glioblastoma. Genes Dev. *29*, 1203–1217.

Liu, F., Hon, G.C., Villa, G.R., Turner, K.M., Ikegami, S., Yang, H., Ye, Z., Li, B., Kuan, S., Lee, A.Y., et al. (2015). EGFR mutation promotes glioblastoma through epigenome and transcription factor network remodeling. Mol. Cell *60*, 307–318.

Mack, S.C., Hubert, C.G., Miller, T.E., Taylor, M.D., and Rich, J.N. (2015). An epigenetic gateway to brain tumor cell identity. Nat. Neurosci. *19*, 10–19.

Pastrana, E., Cheng, L.C., and Doetsch, F. (2009). Simultaneous prospective purification of adult subventricular zone neural stem cells and their progeny. Proc. Natl. Acad. Sci. USA *106*, 6387–6392.

Sanai, N., Alvarez-Buylla, A., and Berger, M.S. (2005). Neural stem cells and the origin of gliomas. N. Engl. J. Med. *353*, 811–822.

Sanai, N., Nguyen, T., Ihrie, R.A., Mirzadeh, Z., Tsai, H.H., Wong, M., Gupta, N., Berger, M.S., Huang, E., Garcia-Verdugo, J.M., et al. (2011). Corridors of migrating neurons in the human brain and their decline during infancy. Nature *478*, 382–386.

Singh, S.K., Hawkins, C., Clarke, I.D., Squire, J.A., Bayani, J., Hide, T., Henkelman, R.M., Cusimano, M.D., and Dirks, P.B. (2004). Identification of human brain tumour initiating cells. Nature *432*, 396–401.

Suva, M.L., Rheinbay, E., Gillespie, S.M., Patel, A.P., Wakimoto, H., Rabkin, S.D., Riggi, N., Chi, A.S., Cahill, D.P., Nahed, B.V., et al. (2014). Reconstructing and reprogramming the tumor-propagating potential of glioblastoma stem-like cells. Cell *157*, 580–594.

Tsankova, N.M., and Canoll, P. (2014). Advances in genetic and epigenetic analyses of gliomas: a neuropathological perspective. J. Neurooncol. *119*, 481–490.

Verhaak, R.G., Hoadley, K.A., Purdom, E., Wang, V., Qi, Y., Wilkerson, M.D., Miller, C.R., Ding, L., Golub, T., Mesirov, J.P., et al. (2010). Integrated genomic analysis identifies clinically relevant subtypes of glioblastoma characterized by abnormalities in PDGFRA, IDH1, EGFR, and NF1. Cancer Cell *17*, 98–110.

Weickert, C.S., Webster, M.J., Colvin, S.M., Herman, M.M., Hyde, T.M., Weinberger, D.R., and Kleinman, J.E. (2000). Localization of epidermal growth factor receptors and putative neuroblasts in human subependymal zone. J. Comp. Neurol. *423*, 359–372.

Stem Cell Reports, Volume *8*

Supplemental Information

Prospective Isolation and Comparison of Human Germinal Matrix and Glioblastoma EGFR^{+} Populations with Stem Cell Properties

Jessica Tome-Garcia, Rut Tejero, German Nudelman, Raymund L. Yong, Robert Sebra, Huaien Wang, Mary Fowkes, Margret Magid, Martin Walsh, Violeta Silva-Vargas, Elena Zaslavsky, Roland H. Friedel, Fiona Doetsch, and Nadejda M. Tsankova

Figure S1 (Relates to Figure 1 and Figure 2)

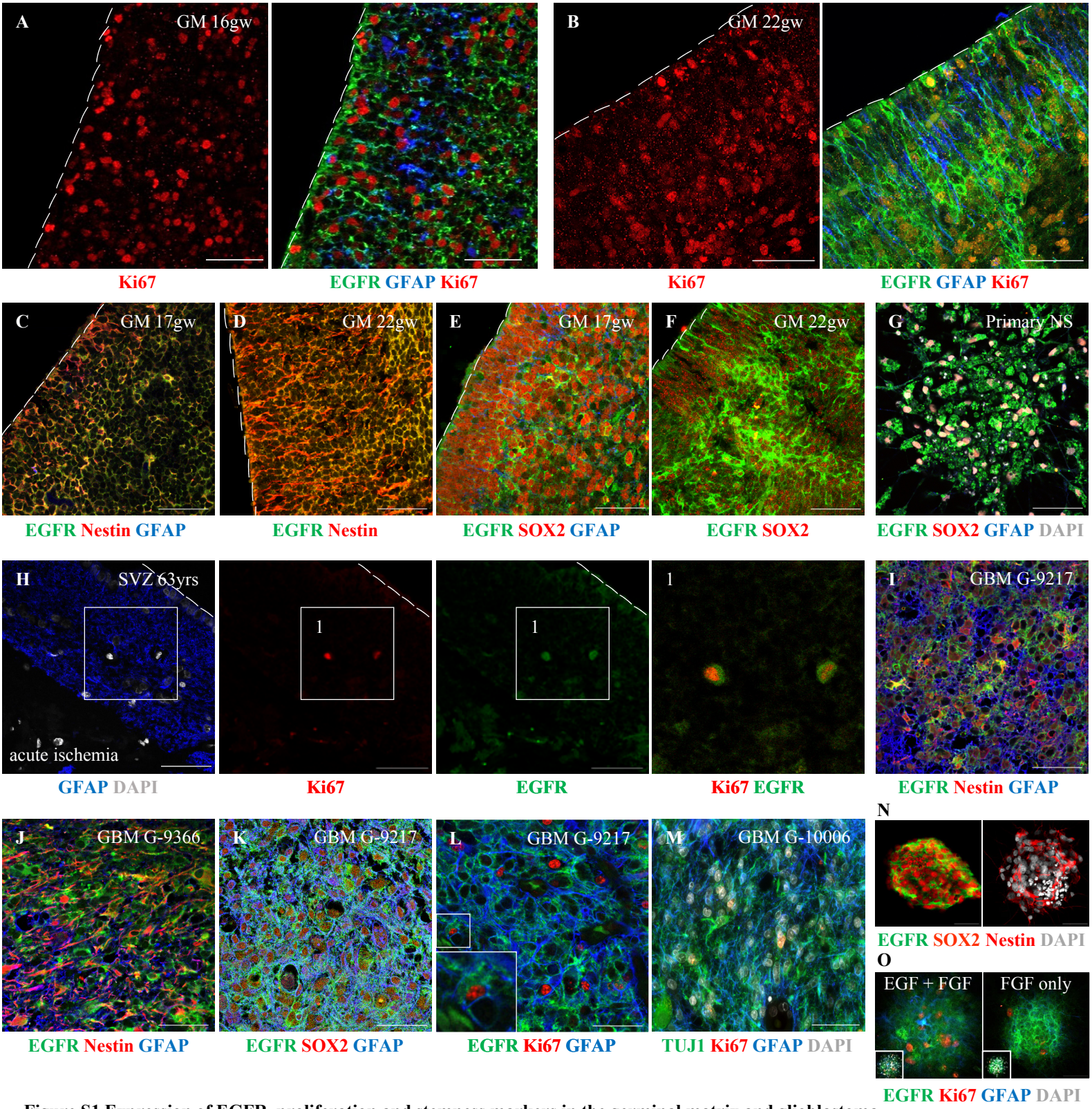

Figure S1 Expression of EGFR, proliferation and stemness markers in the germinal matrix and glioblastoma

Immunofluorescence analysis of EGFR expression in germinal matrix (GM) tissue at 16 and 22 gestational weeks (gw) reveals (**A-B**) active proliferation, as assessed by Ki67, in many EGFR+ but also in EGFR– cells (see also Figure 1A). Most EGFR+ cells in the GM co-express the stem cell markers Nestin (**C-D**) and SOX2 (**E-F**). NESTIN+EGFR– and SOX2+EGFR– cells are also present. (**G**) Single cell-derived clones (1 cell/well) from EGFR+ GM isolates are diffusely positive for EGFR and SOX2, and negative for GFAP. **(H)** Although normally quiescent, cells within the adult SVZ tissue can become reactivated to enter cell cycle after an acute ischemic injury, showing increased EGFR expression and occasional co-localization with Ki67. Immunofluorescence staining of glioblastoma (GBM) tissues (also used for FACS) show frequent co-expression of EGFR with Nestin **(I-J)**, SOX2 **(K),** Ki67 and GFAP **(L)**; as well as variable expression of the neuronal differentiating marker TUJ1 **(M)**. (**N**) Single-cell seeding (1cell/well) of ^{LB}EGFR+DAPI^{low} populations yields GS with diffuse expression of EGFR (ED), SOX2, and Nestin. (**O**) Low-passaged, self-renewing GS grow with and without EGF supplementation in culture, the latter displaying upregulated EGFR expression (10cells/ul, GBM G-12746, ^{LB}EGFR+DAPI^{low} population) . Dashed line indicates ependymal layer. Scale bar: 50µm

Figure S2 (Relates to Figure 1 and Figure 2)

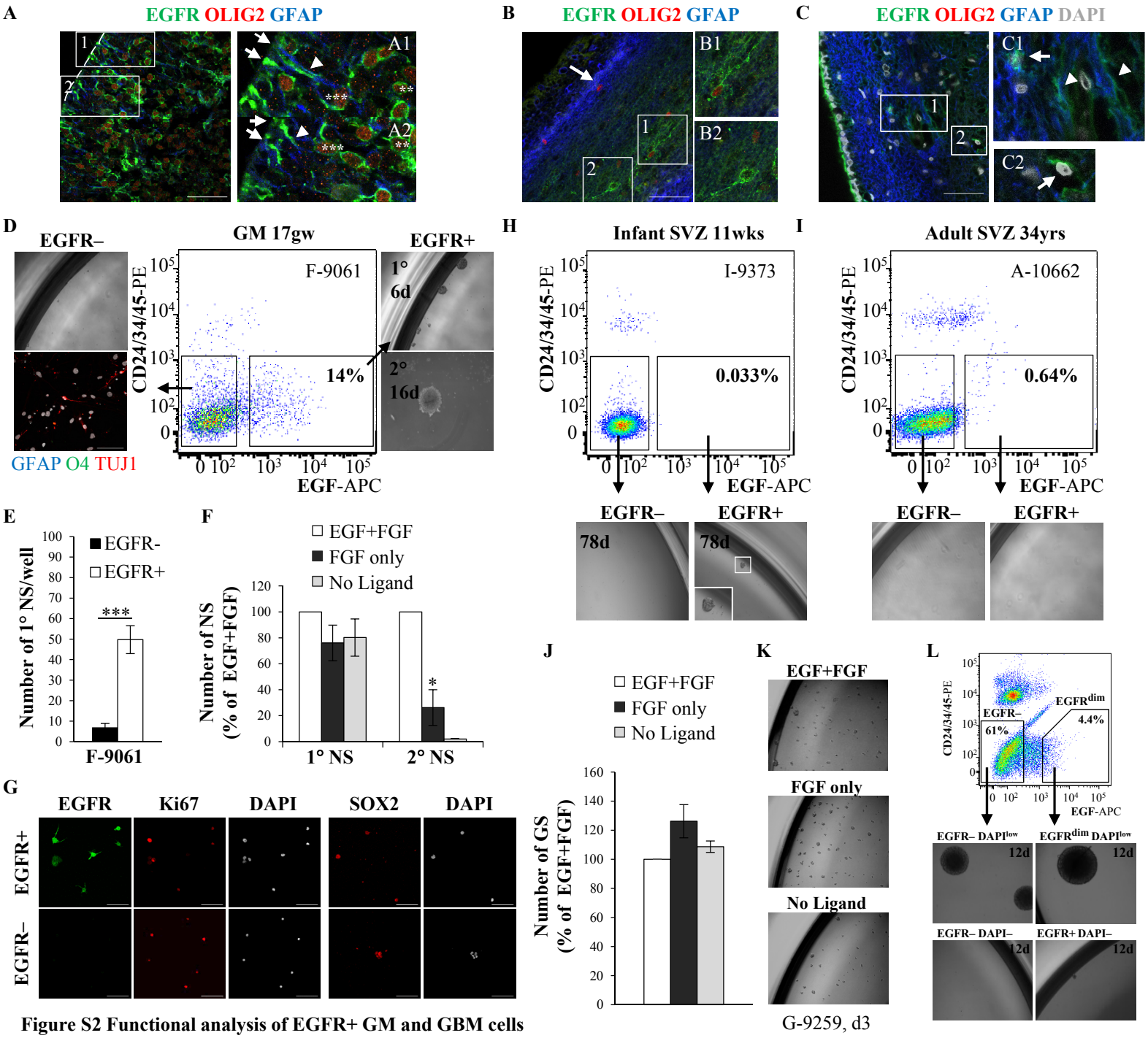

Figure S2 Functional analysis of EGFR+ GM and GBM cells

(A) Immunofluorescence (IF) of GM at 17 weeks of gestation reveals EGFR+ cells with radial morphology (arrows) next to the developing ependymal layer (dash lines) in the lateral ventricle, some of which co-localize with GFAP (arrowhead). Many EGFR+OLIG2+ (**) and scattered EGFR+GFAP+OLIG2+ (***) cells are seen in the deeper GM. **(B)** In the infant SVZ, the expression of EGFR diminishes, but some EGFR+GFAP+, EGFR+OLIG2+ (B1), as well as exclusively EGFR+ (B2) or OLIG2+ (arrow) cells are found. **(C)** Adult SVZ shows occasional EGFR+GFAP+ co-localization in the astrocyte ribbon (C1, arrow) and in the hypocellular layer (arrowheads); EGFR+GFAP– cells are also seen (C2, arrow). **(D-E)** FACS-isolated EGFR+ GM cells form primary (1°) and secondary (2°) neurospheres (NS). Rare 1° NS derived from EGFR– cells were noted in one case of early gestational age, F-9061, in much lower numbers than those derived from EGFR+ cells ($p=0.0009$) ($n=3$); these failed to form 2° NS or to differentiate effectively, undergoing apoptosis with rare TUJ1+ cells and no appreciable GFAP and O4 positivity. **(F)** While 1° NS formation from GM EGFR+ cells is not significantly affected by the withdrawal of EGF or FGF from the cell culture media, 2°NS are reduced ($p=0.03$) ($n=3$). **(G)** IF of acutely isolated EGFR+/– GM cells two hours after FACS shows predominant distribution of EGFR in the positive fraction, and comparable expression of Ki67 and SOX2 (F-9449, 21gw). **(H)** Postnatally, rare NS can be seen in EGFR+ cells up to 11 weeks of infancy, smaller in size, and unable to form 2° NS. **(I)** Occasional EGFR+ cells can be acutely isolated from adult SVZ, but they are not able to form NS, regardless of the age of the specimen ($n=10$). **(J-K)** In GBM, sphere-forming ability is retained in serially passaged GS after removal of EGF ligand ("FGF only") and after removal of all ligands ("No Ligand") from the culture medium ($n=5$). **(L)** GBM tumor, which lacked EGFR amplification, chromosome 7 polysomy, and EGFR expression, did not have a well-defined EGFR+DAPI^{low} population (EGFR^{dim}) and showed equivalent GS formations in the EGFR– and EGFR^{dim} fractions. gw=gestational weeks; wks=weeks, yrs=years; d=days. Percentages of populations shown in FACS plots are from total live events, as determined by DAPI staining. Scale bar=50μM.

Figure S3 (Relates to Figure 2)

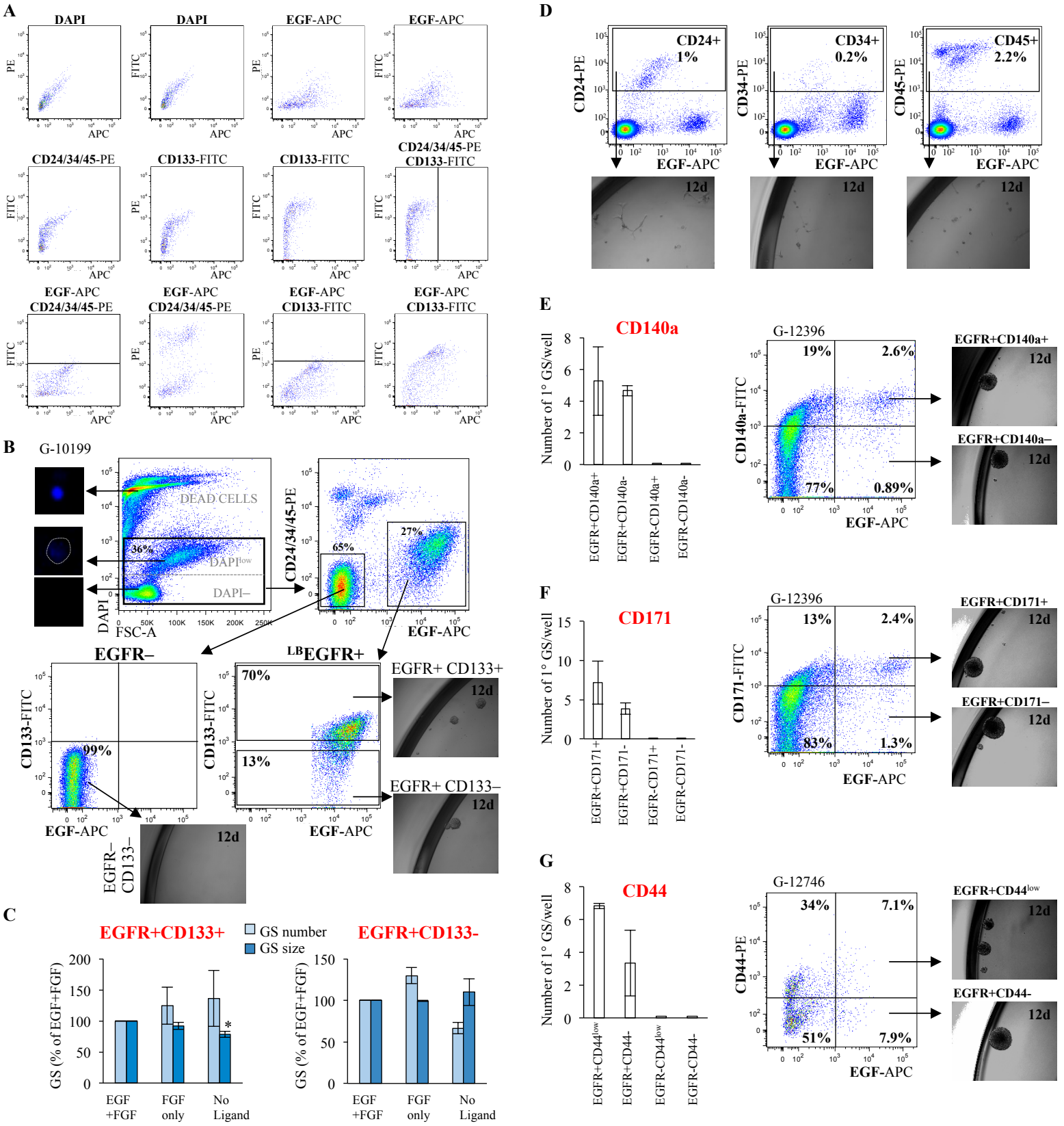

Figure S3 Comparison of EGF ligand and antibody-based isolation of sphere-forming populations in GBM

(A) Representative single and FMO color controls in combined CD133/EGF FACS. **(B)** In GBM, FACS isolation using EGF demonstrates a unique live cell population with forward scatter shift, which is able to incorporate some DAPI (termed DAPI^{low}; dashes outline nucleus). Combined CD133 and EGF FACS analysis demonstrates three defined populations: EGFR+CD133+, EGFR+CD133–, and EGFR–CD133–. Both EGFR+CD133+ and EGFR+CD133– cells display 1° GS formations *in vitro* (day 12, EGF+bFGF) (see also Figure 2I-K). **(C)** EGFR+CD133+ and EGFR+CD133– sorted populations show similar number of GS when grown with or without EGF supplementation, and even with no ligand in the culture medium. EGFR+CD133+ GS formed in no ligand conditions have smaller diameter compared to EGF+FGF (low-passaged, patient-derived GS, n=3 tumors; 6 days). **(D)** CD24+, CD34+, and CD45+ single populations do not form GS (3 tumors, 12 days). **(E-G)** Functional analysis of populations derived from combined FACS using EGF and either CD140a (PDGFRalpha) (n=3) (E), CD171 (n=3) (F), or CD44 (n=2) (G) shows that in each case the ^{LB}EGFR+ populations encompass all sphere-forming cells, including those that lack CD140a, CD171, and CD44 (12 days).

Figure S4 (Relates to Figure 4)

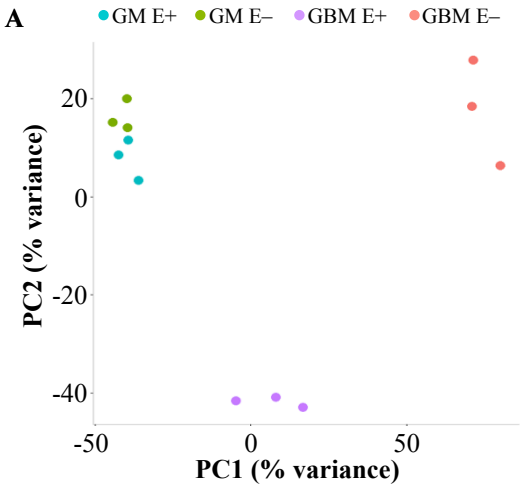

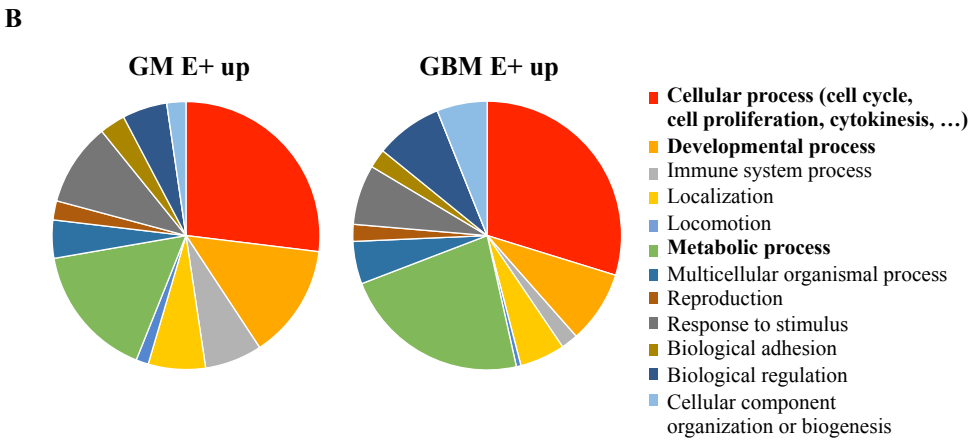

C

GM EGFR+ *vs* EGFR– up (GM E+ up)

TermID	Term	logP
GO:0045880	Positive regulation of smoothened signaling p.	-10.4
GO:0048568	Embryonic organ development	-9.5
GO:0007346	Regulation of mitotic cell cycle	-5.8
GO:0008284	Positive regulation of cell proliferation	-5.8
GO:0005006	EGF-activated receptor activity	-4.9
GO:2000648	Positive regulation of stem cell proliferation	-4.5
GO:0090068	Positive regulation of cell cycle process	-3.9
WP47	Hedgehog signaling pathway	-6.2
WP61	Delta-Notch signaling pathway	-3.5

GM EGFR– *vs* EGFR+ up (GM E+ down)

TermID	Term	logP
GO:0007399	Nervous system development	-17
GO:0007275	Multicellular organismal development	-15.6
GO:0001764	Neuron migration	-14.3
GO:0048856	Anatomical structure development	-14.1
GO:0050808	Synapse organization	-14.0
GO:0048468	Cell development	-12.9
GO:0030182	Neuron differentiation	-12.5
WP2267	Synaptic vesicle pathway	-8.8

D

GBM EGFR+ *vs* EGFR– up (GBM E+ up)

TermID	Term	logP
GO:0000278	Mitotic cell cycle	-67.6
GO:0007059	Chromosome segregation	-32.0
GO:0051726	Regulation of cell cycle	-25.4
GO:0044843	Cell cycle G1/S phase transition	-18.2
GO:0060828	Regulation of canonical Wnt pathway	-8.4
GO:2000648	Positive regulation of stem cell proliferation	-7.9
GO:0005006	EGF-activated receptor activity	-5.5
GO:0031572	G2 DNA damage checkpoint	-4.9
WP47	Hedgehog signaling pathway	-10.7

GBM EGFR– vs EGFR+ up (GBM E+ down)

TermID	Term	logP
GO:0007154	Cell communication	-30.2
GO:0002376	Immune system process	-28.5
GO:0032879	Regulation of localization	-26.1
GO:0030334	Regulation of cell migration	-19.1
GO:0021782	Glial cell development	-8.9
GO:0045597	Positive regulation of cell differentiation	-7.1
WP306	Focal Adhesion	-9.4
WP453	Inflammatory Response Pathway	-6.0

Differential gene expression and gene set enrichment analyses in GM and GBM

(A) Principal component analysis and hierarchical clustering (see Figure 4A) of all RNAseq samples confirms reproducibility, showing a tight clustering of biological replicates. While developing GM EGFR+ and EGFR– transcriptomes are similar to one another, GBM EGFR+ transcriptomes are more similar to GMs than to their EGFR– neoplastic counterpart. **(B-D)** Gene enrichment analyses are performed on the sets of most highly differentially regulated genes (FDR adjusted p ≤0.05, $|\text{Log}_2(\text{fold change})| \geq 2$) in GM EGFR+ *vs*. EGFR– and in GBM EGFR+ *vs*. EGFR–. **(B)** Analysis of differentially upregulated gene sets in EGFR+ GM (GM E+ up) and in EGFR+ GBM (GBM E+ up) using the PANTHER tool depicts prominent representation of top biological processes related to cellular process (cell cycle, cell proliferation, cytokinesis, chromosome segregation, cellular component movement, and cell communication), metabolic process, and developmental process in both data sets. **(C-D)** Analysis for gene set enrichment using the HOMER tool (p ≤0.05, $|\text{Log}_2(\text{fold change})| \geq 2$) in both differentially upregulated (E+ up / E– down) and downregulated (E+ down / E– up) GM and GBM gene sets. Representative top biological and molecular processes (GO) and Wikipathways (WP) are depicted, showing enrichment for cell division, cell cycle regulation, stem cell proliferation, and EGFR signaling in EGFR+ populations of both GM (C) and GBM (D) (top), and more variable processes related to cell differentiation, migration, and inflammation in EGFR– populations (bottom).

Supplemental Table 1 (Relates to Figures 1-4)

Sample information

Sample ID	Sample Type, Age, Sex (Ordered by age)	% Live Cells	% EGFR+ cells	PMT	*In vitro* NS assays	Acute Immunofluorescence	EGF / FGF exclusion	ELDA (stem cell frequency)	RNA-seq
Fetal (F)									
F-9061	GM, 17gw, U	45.3	14	12 hrs	✓	✓			
F-10302	GM, 17gw, U	45	1.9	24 hrs	✓			✓	
F-12437	GM, 19gw, F	77	22	72 hrs	✓				✓ (GM2)
F-13759	GM, 18gw, M	52	9	3 hrs	✓		✓	✓	
F-13970	GM, 19gw, U	66	14.5	6 hrs	✓		✓	✓	
F-10929	GM, 20gw, F	96	1	6 hrs	✓		✓		
F-13969	GM, 21gw, U	77	9.8	6 hrs	✓		✓	✓	
F-9449	GM, 21gw, U	8.9	6.1	48 hrs	✓	✓	✓		✓ (GM1)
F-9062	GM, 21gw, F	38.8	2.1	12 hrs	✓	✓			
F-12266	GM, 22gw, F	73	25	<12 hrs	✓				✓ (GM3)
F-11045	GM, 24gw, F	30.8	8.5	<7 hrs	✓		✓	✓	
F-9491	GM, 25gw, M	11.9	1.5	24 hrs	✓				
Infant (I)									
I-8561	SVZ, 3days, M	66.9	2.72	4 hrs	✓				
I-9063	SVZ, 1wk, F	77	0.3	36 hrs	✓				
I-9373	SVZ, 11wks, F	92.4	0.03	24 hrs	✓				
Adult (A)									
A-10661	SVZ, 9yrs, F	78.9	0.1	12 hrs	✓				
A-10662	SVZ, 34yrs, M	90.8	0.64	12 hrs	✓				
A-10663	SVZ, 44yrs, F	78.1	<0.1	14 hrs	✓				
A-8503	SVZ, 57yrs, M	61	<0.1 (600 c)	21 hrs	✓				
A-10664	SVZ, 71yrs, M	72	<0.1	24 hrs	✓				
A-10665	SVZ, 75yrs, F	64.8	0.1	12 hrs	✓				
A-8155	SVZ, 80yrs, M	93	0.14	23 hrs	✓				
A-8751	SVZ, 80yrs, M	86	0.39	7 hrs	✓				
A-10659	SVZ, 84yrs, M	89.9	0.3	24 hrs	✓				
A-10658	SVZ, 94yrs, F	63	<0.1 (600 c)	14 hrs	✓				

Supplemental Table 1 (Continuation)

Sample ID	Sample Type, Age, Sex	% Live Cells	*EGFR* amp / Chr. 7 status	*EGFRvIII* detection	IDH1 status	EGFR expression (IHC)	*In vitro* GS assays	*In vivo* assays	FACS_Other surface markers	EGF / FGF exclusion	ELDA (stem cell frequency)	RNA-seq
G-9217	GBM, 76yrs, M	93	Amp+ diffuse	Y	WT	Y	✓					
G-9259	GBM, 67yrs, F	90	Amp+ focal	Y	WT	Y	✓	✓		✓	✓	
G-9366	GBM, 88yrs, M	83	Amp+ focal	Y	WT	Y	✓					
G-10006	GBM, 76yrs, M	76	Amp+ focal	Y	WT	Y	✓					✓ (GBM2)
G-10199	GBM, 55yrs, M	36	Amp+ diffuse	Y	WT	Y	✓		✓			
G-10719	GBM, 55yrs, F	84	Amp+ diffuse	Y	WT	Y	✓					
G-11039	GBM, 69yrs, M	90	Amp+ multifocal / Chr.7 Polysomy	Y	WT	Y	✓			✓	✓	
G-11074	GBM, 77yrs, F	75	Amp+ diffuse	Y	WT	Y	✓	✓				
G-11075	GBM, 62yrs, F	96	Chr.7 Polysomy	N	WT	Y	✓	✓	✓	✓	✓	
G-11314	GBM, 58yrs, M	76	Amp+ multifocal	Y	WT	Y	✓	✓	✓	✓		
G-11592	GBM, 39yrs, F	67	Chr.7 Polysomy	N	Mutant	Y	✓				✓	
G-11846	GBM, 49yrs, M	99	Amp+ diffuse	Y	WT	Y	✓					✓ (GBM1)
G-12022	GBM, 81yrs, M	86	Chr.7 Polysomy	N	WT	Y	✓					
G-12048	GBM, 64yrs, F	98	Amp+ diffuse	Y	WT	Y	✓					✓ (GBM3)
G-12396	GBM, 72yrs, M	69	Amp+ diffuse	N	WT	Y	✓		✓			
G-12746	GBM, 60yrs, M	60	None	N	WT	Y	✓		✓	✓	✓	
G-13063	GBM, 69yrs, F	50	None	N	WT	Y			✓	✓	✓	
G-13181	GBM, 73yrs, F	76	None	N	WT	Y	✓’			✓	✓	
G-13306	GBM, 71yrs, M	71	Chr.7 Polysomy	N	WT	Y	✓’			✓	✓	
G-13629	GBM, 69yrs, M	80	Chr.7 Polysomy	N	WT	Y	✓’		✓			
G-10416	GBM, 78yrs, F	81	None	N	WT	N	✓’					
G-11702	GBM, 67yrs, F	80	None	N	WT	N	✓’					

De-identified information for postmortem fetal (F), infant (I), and adult (A) samples, and for glioblastomas (G), used in the various experiments, including code, age, gender, % live cells isolated by fluorescence-activated cell sorting (FACS) assessed by DAPI, % EGFR+ live cells and postmortem time (PMT) (for non-neoplastic only), and EGFR gene amplification (CISH), EGFRvIII mutation (RT-qPCR), IDH1-R132H mutation (IHC), and EGFR expression status (IHC, for tumors only). FACS analysis was performed in all samples, but due to limited surgical and viable postmortem tissue availability, other experiments had more restricted sample allocation. (M = male; F = female; U = unknown gender; gw = gestational weeks; yrs = years; wks = weeks; GM = germinal matrix; SVZ = subventricular zone; c = cells; WT = wild type; Amp = amplification; Chr = chromosome; CISH = Chromogenic In Situ Hybridization; IHC = Immunohistochemistry; ’not included in GS quantification; Y = Yes, N = No).

Supplemental Table 2 (Relates to Figures 1-2)

Analysis of stem cell frequency in GM and GBM

SAMPLE ID	TISSUE TYPE	FACS EGFR+	STEM CELL FREQUENCY (%)		
			EGF+FGF (E+F)	FGF only (F)	No ligands (NL)
F-10302	GM	1° GS	4.0		
F-11045	GM	1° GS	16		
F-13759	GM	1° GS	4.5	4.0	3.0
F-13969	GM	1° GS	22.6	20.3	10.4
F-13970	GM	1° GS	37.7	32.7	25.9
G-11039	GBM	1° GS	3.6		
G-11075	GBM	1° GS	5.5		
G-11347	GBM	1° GS	5.7		
G-9259	GBM	lp GS	30	46	32.7
G-12746	GBM	lp GS	1.9	1.9	
G-13063	GBM	lp GS	22.9	13.7	9.3
G-13181	GBM	lp GS	9	4.3	2.0
G-13306	GBM	lp GS	6.8	7.8	8.2
			Un-paired T-test (p-value) GBM vs. GM		
			E+F	**F**	**NL**
			0.36	**0.74**	**0.99**

TTEST		
Un-paired T-test (p-value) GM		
E+F vs. F	**E+F vs. NL**	**F vs. NL**
0.85	**0.70**	**0.61**
Un-paired T-test (p-value) GBM		
E+F vs. F	**E+F vs. NL**	**F vs. NL**
0.61	**0.74**	**0.88**

Extreme limited dilution assay (ELDA) analysis of primary (1°) and low-passaged (lp) spheres reveals comparable stem cell frequency in EGFR+DAPI– germinal matrix (GM) and ^{LB}EGFR+DAPI^{low} GBM cells, with the ability of both to generate clonal NS/GS from single cells. Un-paired t-test analysis shows no significant difference in stem cell frequency between GBM and GM EGFR+ populations, including under different ligand supplementation conditions: EGF+FGF (E+F), FGF only (FGF), or in absence of both ligands (No ligands, NL).

Supplemental Table 3 (Relates to Figure 4)

Gene enrichment analysis of differentially expressed EGFR+ GM and GBM genes

Whole transcriptome analysis via RNAseq was performed on 3 GBM ^{LB}EGFR+/EGFR– and 3 GM EGFR+/EGFR– acutely sorted populations. After mapping data to the hg38 genome, differential expression analysis was performed between ^{LB}EGFR+ and EGFR– GBM samples, and between EGFR+ and EGFR– GM samples (see also Figure S4 and supplemental experimental procedures). The data was analyzed for gene set enrichment using the HOMER tool (Heinz et al., 2010) (FDR adjusted $p \leq 0.05$, $Log_2(2)$), including analysis of biological processes, molecular functions, wikipathways, and the COSMIC mutation (Forbes et al., 2015) database gene sets. Also included is the list of 50 differentially upregulated genes shared between GM and GBM EGFR+ populations (see also Figure 4C).

Supplemental Experimental Procedures

Sample collection

All specimen collection was performed in accordance with the policies and regulation of the Icahn School of Medicine at Mount Sinai and its institutional review board. For non-neoplastic studies (IRB exemption HS#14-

01007), GM or SVZ were carefully dissected from fresh de-identified pediatric or adult postmortem brains, with comparable representation of either sex, post mortem time < 24 h for adult and < 48 h for pediatric, and without gross brain pathology. One portion of the tissue was placed in fresh PIPES solution for subsequent FACS analysis and cell culture; another portion was frozen on dry ice for downstream molecular analyses; and the remainder was fixed in 4% paraformaldehyde (PFA) for 24-72hrs. For glioma studies (IRB AAAJ9652-Y1M00, HS14#01007), de-identified GBM samples were obtained from the tissue biorepository, within 0.5-3 hours of neurosurgical resection. Only tumor specimens with histological features of GBM on frozen section, evaluated by another neuropathologist, were used for downstream molecular analyses in this study. Refer to Table S1 for additional sample information.

Fluorescence-activated cell sorting

Fresh tissue (~500mg of dissected GM/SVZ and 50-500mg GBM) was first finely minced mechanically, then enzymatically dissociated with papain (Worthington, LS003119, 0.3mg/ml, 45 units/sample) at 37°C for 13 min in rotation, and finally triturated in DMEM media with DNase (Worthington, LS002139, 0.1mg/ml) and ovomucoid protease inhibitor (Sigma Aldrich, 0.7mg/ml). Extracellular debris and myelin were removed by passage through 22% Percoll; red blood cells were lysed for 10min at RT (Ebioscience, 00-4300-54); then cells were washed once with HBSS+1% BSA+0.1% glucose. Live cell number was calculated via trypan blue incorporation using an automated cell counter (Countess, Invitrogen). Cells were incubated with Alexa Fluor® 647 (APC) EGF complex (Life Technologies, E-35351) (1μg/10^6 live cells) for 30 min on ice. In some experiments, antibodies against CD133-FITC, CD171-FITC, CD140a-FITC, and CD44-PE were used in combination with EGF. Exclusion of ependyma/neuroblasts, endothelium, and inflammatory cells were accomplished with CD24-PE, CD34-PE, CD45-PE, respectively (Codega et al., 2014). DAPI was used to discern between live and dead cells. No color, single color, and fluorescence minus one (FMO) color controls were done to establish negative/positive cut-off values for the populations. Cells were sorted on a Becton Dickinson FACSAria™ III sorter. See antibody summary below.

Self-renewal, differentiation, and ELDA protocols

For primary NS/GS formation analysis, immediately after sorting, cells were seeded on 96-well low-adherence plates at a density of 10c/μl, in triplicates, in NS media (1X N2, 1X B27, 20μM glutamine, 1X Insulin/Transferrin/Selenium, 15mM HEPES, 0.6% glucose, 1X Antibiotic/Antimycotic, in DMEM/F12 media) supplemented with EGF (20ng/ml) and bFGF (20ng/ml) (FGF). In some cases, EGF and/or bFGF was omitted. Cells were maintained at 37°C and 5% CO_2 for up to 4 weeks, changing 2/3 of media after day 6^{th} and every 3-4 days thereafter. For acute staining analysis, 2000 EGFR– and EGFR+ cells were seeded immediately after FACS isolation on PDL-laminin-coated coverslips, incubated at 37°C for 2hr in NS media without growth factors, then gently centrifuged for 1min at 1000rpm, fixed for 10min with 4% PFA, washed with 1X PBS, and stored at 4°C for IF. The rest of the sorted cells were pelleted at 500g for 5min at 4°C and immediately frozen at -80°C for subsequent DNA/RNA analyses. Images of NS/GS formation were captured with a light inverted microscope (Motic AE31) at Day6, Day12, and Day25 after seeding. Pictures covering the entire surface of the wells were taken at 10X and were used for subsequent counting. NS/GS diameter size was measured in all clones of all wells, 3 replicates/sample, and analyzed using ImageJ 1.43u software. For secondary/tertiary sphere passaging, single NS/GS reaching minimum size of 40μM were picked, pelleted at 100g for 1min, dissociated in 1ml of Accumax solution (Innovative Cell Technologies) for 10mins at RT with trituration, and incubated in NS media with growth factors (see above) at a clonal density of 1c/μl ((Pastrana et al., 2011). For differentiation, NS/GS were picked up and seeded on PDL-laminin coated glass coverslips or on 16-well chamber-slides (Thermofisher, 12-565) in differentiating NS media without B27, EGF, and bFGF, incubated for 14 days, and then fixed in 4% PFA for 10mins at RT. For some cases of differentiation O4 analysis, T3 hormone (1:1000) was added every 3 days. In all the experiments cells were seeded in triplicates.

Stem cell (self-renewal) frequency was calculated by using Extreme Dilution Limited Assay (ELDA) (Hu and Smyth, 2009). Briefly, FACS-sorted EGFR+ cells were plated in decreasing numbers from 100 cells/well to 1 cell/well in 200μl in similar conditions as for NS/GS formation analysis. Cultures were maintained until day 25 as described above. Then, the number of wells containing spheres for each cell plating density (number of positive cultures) was recorded, and plotted using online ELDA analysis program (http://bioinf.wehi.edu.au/software/elda).

RNAseq data analysis

Illumina sequencer output FASTQ files for each sample were subjected to a quality control assessment using the FASTQC package. RNAseq reads were aligned to the human genome (GENCODE GRCh38) using STAR with default settings (Dobin et al., 2013). Gene counts were obtained using the featureCount utility of the subread

package (Liao et al., 2014). Differential expression analysis on the RNAseq data was performed using the DESeq2 R package (Love et al., 2014), which models the data with a negative binomial distribution and uses Empirical Bayes shrinkage for dispersion and fold-change estimation. Gene set enrichment analysis was done utilizing the HOMER tool (Heinz et al., 2010). The gene background set for the enrichment analysis was defined as the set of genes passing the independent filtering low expression threshold by DESeq2. All RNAseq tests were FDR adjusted for multiple testing correction.

Gene expression analysis

For bulk tumor, total RNA was isolated using RNA easy mini kit (Qiagen, 71404) with DNase treatment (Qiagen, 79254). For sorted cells, total RNA was isolated via Trizol /chloroform /isopropanol extraction method following manufacturer's instructions (Life Technologies), followed by RNA cleanup-and-concentrator kit with DNase treatment (Zymo Research, R1013). cDNA was generated using the High-Capacity RNA-to-cDNA Kit (Life Technologies, 4387406). qPCR reactions were run in duplicates using the SYBR-Green based system (Quanta Biosciences). Each sample Ct value was normalized against the expression of the 40S Ribosomal Protein S11 (*RPS11*) as a housekeeping gene (HKG). Data was expressed either as the exponential fraction of HKG expression levels $2^{-(CtSample - CtHKG)}$ ($2^{-\Delta Ct}$) or as a fold change relative to the EGFR– fractions ($2^{-\Delta\Delta Ct}$). All primers used for the reactions (see table below) were designed to span exon-exon junctions in order to minimize genomic contamination except for those ones with no introns in their DNA sequence. Melting curves were analyzed to ensure specificity of the primers for a single product, and product size was confirmed by 2% agarose gel electrophoresis.

Table summary of primers used for RT-qPCR analysis

GENE	**Forward (5'-3')**	**Reverse (5'-3')**
ASCL1	GGACTTTGGAAGCAGGGTG	CGCCACTGACAAGAAAGCA
CENPE	TTCAGCCTGATAGGATGGCG	TTGGGCAGTTTCTCCAAGTGA
DBF4	GGACATTAAGGATCTGGGAGGG	TTGTGCAAATTTAGCTTCCTTCT
EGFR exons 17-18	GATCGGCCTCTTCATGCGA	GTAAGAGGCTCCACAAGCTCC
EGFR exons 3-4	TCCAGGAGGTGGCTGGTTAT	ACGGCGCCATGCAGGAT
EGFRvIII exons 1/8	GGCTCTGGAGGAAAAGAAAGGTAA	CAAGGCCCTTCGCACTTCTTA
KNSTRN	GAGCTGCTGGAGAAGTTTCG	CCAGGGTCTCACTGCCTAAAG
KPNA2	AGCTCCAAGCTACTCAAGCTG	CCAGCCCGGATTATGTTGTCT
HKG	**Forward (5'-3')**	**Reverse (5'-3')**
RPS11	ATGTCCAGCCTCAGAACTTC	GCCGAGACTATCTGCACTAC

Orthotopic transplantation

All procedures performed in studies involving animals were in accordance with the ethical standards of the Icahn School of Medicine at Mount Sinai (ISMMS). FACS-sorted cell populations from GBM samples (^{LB}EGFR+DAPI^{low}, ^{LB}EGFR+DAPI–, EGFR–DAPI^{low}, or EGFR–DAPI–) without prior culturing were injected into the striatum of 2-month-old male mice with B & T cell ICR-Severe Combined Immunodeficiency (SCID) (IcrTac:ICR-Prkdc^{SCID} strain, Taconic). Microinjections were performed using a stereotactic apparatus (Stoelting) and microsyringe (Hamilton). For each mouse, $1x10^5$ cells were injected in a volume of 2 µl (Opti-MEM, Thermofisher) at the following stereotactic coordinates: 2mm right lateral to Bregma and 3mm deep. Note: for ^{LB}EGFR+DAPI– mice only, $0.5x10^5$ cells were available for injection. After 2 months, mice were sacrificed and tumor initiation was analyzed by histological examination. At later time points, additional mice were sacrificed if they became clinically symptomatic.

Immunofluorescence/Immunohistochemistry

Specimens were fixed in 4% paraformaldehyde (PFA) in phosphate buffered saline (1X PBS) for 24hr (SVZ) to 72hr (GM) at 4°C, or in 10% formalin/1X PBS for 1-15 days (GBM and some GM and SVZ cases). Floating

vibratome sections (40-60µm, stored in 1X PBS /0.01% NaN3) and formalin-fixed paraffin-embedded (FFPE) sections (4µm) were used. Mice were anesthetized with pentobarbital (i.p. injection of 650 mg/kg) and transcardially perfused with 1X PBS first and then with 4% PFA/1X PBS. Brains were removed and post-fixed in 4% PFA/1X PBS overnight, cryoprotected in sucrose gradient, and then embedded in O.C.T. Brains were serially cut with a cryostat (25µM). For immunofluorescence (IF) experiments, FFPE and vibrotome sections underwent antigen retrieval in boiling citrate buffer pH6 (Vector labs), blocking (10% normal donkey serum (NDS)/0.5% triton-X (TX), 1hr at RT), primary antibody incubation (1% NDS/0.25% TX overnight at 4°C), and species-appropriate fluorochrome-conjugated secondary antibody incubation (1% NDS/0.25% TX for 4hr at RT). Nuclear counterstain was with DAPI. For EGFR IF of adult SVZ, the primary antibody signal was amplified with TSA amplification system (PerkinElmer Labs, NEL700A001KT). Briefly, enzymatic digestion of the tissue was performed with protease enzyme (10µg/ml) at 37°C for 10min followed by 10min at RT. After blocking in TNB buffer for 30min at RT, sections were incubated with primary monoclonal mouse EGFR antibody (Invitrogen) overnight at 4°C. Secondary anti-mouse HRP-conjugated antibody was incubated for 4h at RT and one cycle of amplification was performed with tyramide and FITC-conjugated Streptavidin following manufacturer's instructions. Pertinent negative controls were simultaneously performed to ensure specific signal. FFPE sections were processed similarly to vibratome sections, with the exception of 1hr deparaffinization with subsequent rehydration in decreasing gradient of ethanol, antigen retrieval for 20min, blocking in 5% NDS/0.5% TX for 30min. IF on cells, mouse brain tissue, or differentiated NS/GS were performed similarly to human vibrotome tissues, except for omitting antigen retrieval and signal amplification. Specifically, O4 IF was performed on live unfixed cells, incubated with primary and secondary antibodies for 40min at 4°C and later fixed with 4% PFA. Zeiss LSM710 confocal microscope was used for visualization. Acute IF staining was performed similarly to NS/GS, except with 0.5hr blocking and 2hrs secondary antibody incubation. All immunohistochemical and EGFR chromogenic in situ hybridization (CISH) experiments were performed on automated Ventana XT/ULTRA machines following standard protocols (Ventana). Immunoreactivity was detected by means of the ultraview universal DAB detection kit (Ventana, 760-500) or ultraview SISH DNP detection kit (Ventana, 760-098).

Table summary of antibodies used for immunofluorescence and FACS

ANTIBODY	COMPANY	CATALOG NUMBER	DILUTION
Mouse anti-EGFR ED	INVITROGEN	280005	1:50
Rabbit anti-EGFR ID	MILLIPORE	06-847	1:50
Rat anti-GFAP	LIFE TECHNOLOGIES	13-0300	1:1000
Mouse anti-human GFAP	CELLARTIS	Y40420	1:500
Mouse anti-HNA	MILLIPORE	MAB1281	1:400
Rabbit anti-Ki67	ABCAM	Ab15580	1:250
Mouse anti-Nestin	MILLIPORE	MAB5326	1:250
Mouse anti-O4	MILLIPORE	MAB345	1:200
Rabbit anti-OLIG2	MILLIPORE	AB9610	1:250
Rabbit anti-SOX2	STEMCELL TECHNOLOGIES	60055	1:100
Mouse anti-TUJ1	BIOLEGEND	MMS-435P	1:500
Rabbit anti-TUJ1	COVANCE	PRB-435P	1:1000
EGF ligand-AF647 conjugated	LIFE TECHNOLOGIES	E-35351	1:200
Anti-CD24 PE-conjugated	BD BIOSCIENCES	560991	1:10
Anti-CD34 PE-conjugated	BD BIOSCIENCES	550619	1:10
Anti-CD45 PE-conjugated	BD BIOSCIENCES	555483	1:10
Anti-CD24 FITC-conjugated	BD BIOSCIENCES	560992	1:10
Anti-CD34 FITC-conjugated	BD BIOSCIENCES	560942	1:10
Anti-CD45 FITC-conjugated	BD BIOSCIENCES	560976	1:10
Anti-CD133 Biotin-conjugated	MILTENYI BIOTEC	130-090-664	1:10
Anti-CD44 PE-conjugated	BD BIOSCIENCES	550989	1:10
Anti-CD140a Biotin-conjugated	BIOLEGEND	323503	2µg/10^6 cells
Anti-CD171 Biotin-conjugated	MILTENYI BIOTEC	130-100-703	1:11
Donkey anti-Mouse AF488 conjugated	JACKSON IMMUNORESEARCH	715-545-151	1:250

Donkey anti-Rabbit Cy3 conjugated	JACKSON IMMUNORESEARCH	711-165-152	1:250
Donkey anti-Rat AF647 conjugated	JACKSON IMMUNORESEARCH	712-605-153	1:500
Donkey anti-Mouse Cy3 conjugated	JACKSON IMMUNORESEARCH	715-165-151	1:500
Donkey anti-Rabbit AF488 conjugated	JACKSON IMMUNORESEARCH	711545152	1:500
IgM anti-Mouse-AF488	JACKSON IMMUNORESEARCH	115-545-075	1:500
IgM anti-Mouse-AF568	MOLECULAR PROBES	A-21043	1:500
DyLight 488 Streptavidin	VECTOR LABS	SA-5488-1	1:250
EGFR-CISH probe	VENTANA	760-1216	-
Chromosome 7-CISH probe	VENTANA	760-1219	-

Statistical analysis

Two-tailed unpaired Students' t-test was used to calculate significance (*$p \leq 0.05$, **$p \leq 0.01$, ***$p < 0.001$), which was corrected for non-homogeneous variances. For non-parametric analysis, we used the Mann-Whitney U test. Bar graph data is represented as mean ± SEM except for bar graphs in Figure 4E where plots show the median (black horizontal line), 25th and 75th percentiles (boxes) and range (whiskers) of the data. All pooled data in the main and supplementary figures comes from independent experiments, except for Figure S2E (3 wells from one sample).

References

Codega, P., Silva-Vargas, V., Paul, A., Maldonado-Soto, A.R., Deleo, A.M., Pastrana, E., and Doetsch, F. (2014). Prospective identification and purification of quiescent adult neural stem cells from their in vivo niche. Neuron *82*, 545-559.

Dobin, A., Davis, C.A., Schlesinger, F., Drenkow, J., Zaleski, C., Jha, S., Batut, P., Chaisson, M., and Gingeras, T.R. (2013). STAR: ultrafast universal RNA-seq aligner. Bioinformatics *29*, 15-21.

Forbes, S.A., Beare, D., Gunasekaran, P., Leung, K., Bindal, N., Boutselakis, H., Ding, M., Bamford, S., Cole, C., Ward, S.*, et al.* (2015). COSMIC: exploring the world's knowledge of somatic mutations in human cancer. Nucleic acids research *43*, D805-811.

Heinz, S., Benner, C., Spann, N., Bertolino, E., Lin, Y.C., Laslo, P., Cheng, J.X., Murre, C., Singh, H., and Glass, C.K. (2010). Simple combinations of lineage-determining transcription factors prime cis-regulatory elements required for macrophage and B cell identities. Molecular cell *38*, 576-589.

Hu, Y., and Smyth, G.K. (2009). ELDA: extreme limiting dilution analysis for comparing depleted and enriched populations in stem cell and other assays. Journal of immunological methods *347*, 70-78.

Liao, Y., Smyth, G.K., and Shi, W. (2014). featureCounts: an efficient general purpose program for assigning sequence reads to genomic features. Bioinformatics *30*, 923-930.

Love, M.I., Huber, W., and Anders, S. (2014). Moderated estimation of fold change and dispersion for RNA-seq data with DESeq2. Genome biology *15*, 550.

Pastrana, E., Silva-Vargas, V., and Doetsch, F. (2011). Eyes wide open: a critical review of sphere-formation as an assay for stem cells. Cell stem cell *8*, 486-498.